Inline $Cu(In,Ga)Se_2$ Co-evaporation for High-Efficiency Solar Cells and Modules

Johan Lindahl, Uwe Zimmermann, Piotr Szaniawski, Tobias Törndahl, Adam Hultqvist, Pedro Salomé, Charlotte Platzer-Björkman, and Marika Edoff

***Abstract*—In this paper, co-evaporation of $Cu(In,Ga)Se_2$ (CIGS) in an inline single-stage process is used to fabricate solar cell devices with up to 18.6% conversion efficiency using a CdS buffer layer and 18.2% using a $Zn_{1-x}Sn_xO_y$ Cd-free buffer layer. Furthermore, a 15.6-cm^2 mini-module, with 16.8% conversion efficiency, has been made with the same layer structure as the CdS baseline cells, showing that the uniformity is excellent. The cell results have been externally verified. The CIGS process is described in detail, and material characterization methods show that the CIGS layer exhibits a linear grading in the [Ga]/([Ga]+[In]) ratio, with an average [Ga]/([Ga]+[In]) value of 0.45. Standard processes for CdS as well as Cd-free alternative buffer layers are evaluated, and descriptions of the baseline process for the preparation of all other steps in the Ångström Solar Center standard solar cell are given.**

***Index Terms*—Buffer layer, Cd-free, $Cu(In,Ga)Se_2$ (CIGS), inline co-evaporation, thin-film solar cells, $Zn_{1-x}Sn_xO_y$.**

TABLE I
SUMMARY OF THE CIGS SOLAR CELL STACK

Layer	Deposition Method	Typical Thickness [nm]	Typical Sheet Resistance [Ω/square]
Mo back contact	DC sputtering	350	0.6
CIGS absorber	Co-evaporation	1700	-
CdS buffer layer	Chemical bath deposition	50	-
$Zn_{1-x}Sn_xO_y$ buffer layer	Atomic layer deposition	13	-
Zn(O,S) buffer layer	Atomic layer deposition	20	-
i-ZnO	RF-sputtering	90	-
ZnO:Al front contact	RF-sputtering	350	30
Ni/Al/Ni grid	Evaporation	3000	0.015

I. Introduction

In-depth grading of Ga has been successfully employed to enhance efficiency in $Cu(In,Ga)Se_2$ (CIGS)-based solar cells. A self-assembled grading is obtained in the so-called three-stage process [1], with a notch in the [Ga]/([Ga]+[In]) ratio. The position and depth of this notch can, at least partly, be engineered by adjusting the respective lengths of the three stages as well as by changing the temperature in the high-temperature stages (i.e., stages 2 and 3). The notch formation has been suggested to be governed by Cu and In interdiffusion [2]. Keeping the [Cu]/([Ga]+[In]) ratio near stoichiometry at all times during the deposition makes it possible to tailor the [Ga]/([Ga]+[In]) ratio through the depth of the solar cell. In a direct comparison between a single-stage and a multistage process in the same evaporation system, the single-stage process led to lower efficiency [3]. In this paper, we show that efficiencies of up to 18.6% can be obtained with an inline deposition process, using a linear gradient with no notch and with a total active deposition time of 17.5 min using three metal sources and with a substrate temperature of 520 °C. The baseline processes, as well as the substrates used, are standard processes that have been developed for reproducibility and robustness and not primarily for highest efficiencies. Some changes that have been employed to enhance robustness are related to thicknesses of buffer layers and window layers as well as avoiding bending of the glass substrates by using relatively low substrate temperatures. In addition, waiting times between the various processes are controlled and minimized.

Similar efficiencies are obtained with buffer layers deposited with atomic layer deposition (ALD) as with the wet chemical deposited CdS buffer, which could enable production without breaking vacuum between CIGS and window layer process steps.

II. Device Processing and Measurements

Table I shows a summary of all the process steps and layers in the current baseline used at the Ångström Solar Center (ÅSC). All layer thicknesses in this paper have been measured with a Veeco Dektak 150 Stylus Profiler, and all sheet resistance measurements have been performed by a CMT-SR2000N four point probe, if not stated otherwise.

A. Substrates

The substrates used in the baseline are either 12.5 cm × 12.5 cm (2 mm thick) or 10 cm × 10 cm (1 mm thick) low-iron soda-lime glasses (SLG). After the CIGS deposition, the samples are usually cut into four parts, and the complete 5 cm × 5 cm devices contain 32 0.5-cm^2 cells.

Before the deposition of the molybdenum back contact, the substrates are submitted to a cleaning process. The glasses

Manuscript received December 10, 2012; revised February 13, 2013; accepted March 21, 2013. Date of publication April 18, 2013; date of current version June 18, 2013. This work was supported by the Swedish Energy Agency and STandUp for Energy.

The authors are with the Ångström Solar Center, Division of Solid State Electronics, Uppsala University, 75121 Uppsala, Sweden (e-mail: johan.lindahl@angstrom.uu.se; uwe.zimmermann@angstrom.uu.se; piotr.szaniawski@angstrom.uu.se; tobias.torndahl@angstrom.uu.se; adam.hultqvist@angstrom.uu.se; pedrosalome@gmail.com; charlotte.platzer@angstrom.uu.se; marika.edoff@angstrom.uu.se).

Color versions of one or more of the figures in this paper are available online at http://ieeexplore.ieee.org.

Digital Object Identifier 10.1109/JPHOTOV.2013.2256232

are immersed into a tank with deionized (DI) water and Cole-Parmer Micro-90 detergent. The tank is heated to 60 °C and, subsequently, put into an ultrasonic bath. After that follows four rinsing steps in 60 °C DI water using ultrasonic agitation. Finally, the substrates are dried in a spin rinse dryer with nitrogen atmosphere.

B. Back Contact

The molybdenum back contact layer is deposited in a vertical inline MRC 603 dc sputtering system using a Mo target with 4N purity. The sputtering pressure and power is 0.8 Pa and 1500 W, respectively, and the substrates pass in front of the target with a speed of 7 cm/min. This results in a Mo layer with a sheet resistance of 0.6 $\pm$ 0.1 Ω/square and a thickness of 350 $\pm$ 20 nm.

C. Cu(In,Ga)Se_2 Absorber

The growth of the CIGS is performed in an inline co-evaporation system pumped with turbomolecular pumps with a base pressure of about 1×10^{-4}Pa. The substrates are mounted individually into vertical metal frames, which are introduced from a load-lock, by a robotic arm, onto a carrousel inside the deposition chamber. The substrates are facing inwards toward the center where the metal sources are situated. The substrates move sequentially through a heating zone, a deposition zone, and a cooling zone. In the heating and deposition zones, the substrates are heated to 520 °C from the backside by means of quartz halogen lamps delivering constant power, while their temperature is monitored by thermocouples and pyrometers. There is room for 24 substrates in the carrousel. The system is constructed so that one full deposition takes about 60 min, whereof the active deposition time is about 17.5 min. This leads to, when the system is run in continuous mode, that one sample can be loaded and another one unloaded every 2.5 min. However, for all the samples in this paper, the rotation speed was increased by a factor of 2 after the sample passed the deposition zone to get less elemental selenium on the CIGS surface.

The substrates pass three single elemental metal sources consisting of pyrolytic boron nitride crucibles heated from outside by means of filaments, in the order, gallium, copper, and indium. The three metal sources are mounted in the middle of the chamber pointing outwards and evaporate horizontally. The sources are held at constant temperatures and controlled by thermocouples in a feedback loop, with accuracy better than ±1 °C. Selenium is evaporated in excess from a source placed at the bottom of the evaporation system. Our experience from running the system shows that the drift in CIGS composition from sample to sample and from run to run is very small. With constant source temperatures and similar source filling heights, the [Cu]/([Ga]+[In]) ratio is 0.90 and the [Ga]/([Ga]+[In]) ratio is 0.45 with run to run [Ga]/([In]+[Ga]) and [Cu]/([In]+[Ga]) variations less than 0.05 on identical positions on each sample, measured by X-ray fluorescence spectrometry (XRF) on a PANalytical Epsilon 5 EDXRF spectrometer setup. Thickness and [Cu]/([In]+[Ga]) and [Ga]/([In]+[Ga]) variations over a single sample are all less than 5%. The typical layer thickness is approximately 1700 $\pm$ 300 nm, between runs, but varies much less within a run.

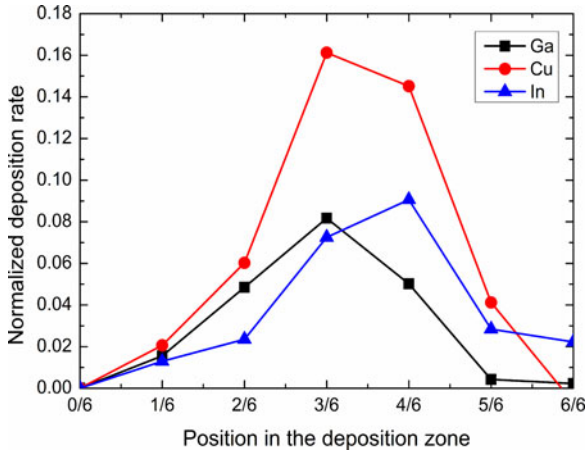

Fig. 1. Estimated deposition rates for Ga, Cu, and In from the six deposition zones in the inline CIGS deposition system.

An experiment was performed to estimate the variation of the evaporation rates (in atomic percent) in the deposition zone, and the results are shown in Fig. 1. The rates are normalized, such that the sum of all points for all elements adds up to unity. For this experiment, temporary shields were mounted between the substrates and the sources in the evaporation zone. Five shields were mounted and removed one by one in six consecutive runs. In the first run, only the first subzone was open, in the second run, the first two subzones were open, and so on until no shields were left. The thickness and composition of the resulting films were measured, and the points in Fig. 1 are obtained by subtracting the XRF values of the partial CIGS films from run $n + 1$ with the values from run n. The diagram shows that the profile is deposited with a built-in [Ga]/([Ga]+[In]) profile since the maximum In rates occur later in the process than the maximum Ga rates. The asymmetry of the In profile is caused by an intentional rotation of that source.

None of the analyzed partly deposited samples showed a copper rich composition; thus, the [Cu]/([Ga]+[In]) ratio was below unity at all times during the evaporation. The average values of composition for all references with the full deposition was the same as in standard runs, i.e., [Cu]/([Ga]+[In]) = 0.90 and [Ga]/([Ga]+[In]) = 0.45.

The elemental depth profiles for Cu, In, Ga, Se, Mo, Na, O, and K were measured using secondary ion mass spectrometry (SIMS) at Evans Analytical Group, where a calibration sample was used to quantify the concentration of those elements in the CIGS layer. Two separate SIMS sputtering runs with oxygen and gallium as primary ions were made for each sample to obtain the concentration profile of both electronegative (Cu, In, Ga, Se, Mo, K, and Na using oxygen) and electropositive (O using gallium) ions. The quantification of the SIMS thickness was performed using stylus profilometry after the SIMS measurement. As Fig. 2 illustrates, the sequential nature of the deposition process results in an almost linear Ga gradient through the thickness of the layer. The [Ga]/([Ga]+[In]) ratio increases

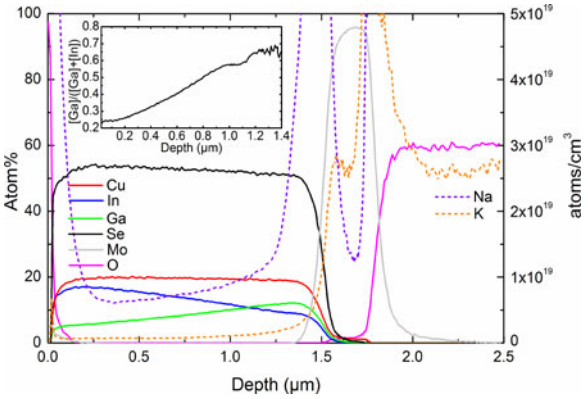

Fig. 2. SIMS depth profile over a baseline device from the CIGS layer down to the glass substrate. Na and K are measured in atoms/cm^3 on the right axis, whereas Cu, In, Ga, Se, Mo, and O are measured in atom percentage on the left axis. The inset shows the [Ga]/([Ga]+[In]) ratio as a function of depth.

from 0.25 at the front to 0.65 toward the back contact, thus forming a back-surface field [2]. This value corresponds reasonably well to what can be calculated from the evaluation of the rate profiles discussed previously. To calculate the bandgap of the $CuIn_{1-x}Ga_xSe_2$ layers, the empirical expression [4]

$$E_g = 1.010 + 0.626x - 0.167x(1-x) \quad (1)$$

where x is the [Ga]/([Ga]+[In]) ratio, can be used. Inserting the [Ga]/([Ga]+[In]) ratios at the front and back contact results in bandgap energies of 1.14 and 1.38 eV.

D. Buffer Layers

A buffer layer is deposited as soon as possible after the samples are brought out in open air, normally within 5 min. This is done to minimize oxidation and other reactions of the CIGS layer that starts to occur as soon as it is exposed to air [5]. The short air exposure time is especially important for alternative buffer layers deposited with the dry ALD technique, which lacks the CIGS surface etching that is a part of the chemical bath deposition (CBD) process due to the presence of ammonia [6]. We currently have established baseline recipes for CdS, Zn(O,S), and $Zn_{1-x}Sn_xO_y$ buffer layers.

1) CdS Buffer Layer: The CdS buffer layer is deposited with a standard CBD process. The CBD bath contains a solution with 1.1 M ammonia, 0.100 M thiourea, and 0.003 M cadmium acetate. The solution is mixed in a beaker at room temperature, and the samples are immersed into the beaker, which is subsequently heated to 60 °C in a water bath. During the growth process, the solution is stirred for 10 s each minute. The baseline process time is 8 min and 15 s, and the samples are then directly moved from the CBD beaker and immersed into a beaker with clean DI water to stop the growth process. This process yields a thickness of 50 nm when grown on CIGS according to transmission electron microscopy.

2) $Zn_{1-x}Sn_xO_y$ Buffer Layer: A process for deposition of an alternative buffer layer of $Zn_{1-x}Sn_xO_y$ by ALD has recently been established by the ÅSC group [7]. The $Zn_{1-x}Sn_xO_y$ buffer layers are deposited in an F-120 Microchemistry ALD reactor at a deposition temperature of 120 °C using diethyl zinc (DEZn or $Zn(C_2H_5)_2$), tetrakis(dimethylamino) tin (TDMASn or $Sn(N(CH_3)_2)_4$), and deionized water 18 MΩ·cm (H_2O) as precursors. Both the water and the diethyl zinc are effused into the chamber at room temperature, whereas the Sn precursor is heated in a water bath to 40 °C to achieve a suitable vapor pressure. The process uses nitrogen gas (N_2, 6N) as a carrier gas. The samples are loaded into the reactor 30 min prior to film deposition for temperature stabilization. Pulse lengths for the ALD Sn or Zn precursor:N_2:H_2O:N_2 pulse cycle are 400:800:400:800 ms, respectively. The [Sn]/([Zn]+[Sn]) composition of the films is controlled by the relative amount of tin or zinc containing precursor pulses. The baseline process uses 500 ALD pulse cycles in total with a Sn/(Zn+Sn) pulse ratio of 0.40. The resulting $Zn_{1-x}Sn_xO_y$ buffer layer when deposited on air exposed CIGS has a thickness of 13 ± 5 nm and a [Sn]/([Zn]+[Sn]) composition of 0.15–0.20 [7].

E. Front Contact

A von Ardenne CS600S radio frequency (RF) horizontal sputtering system, where the substrates are stationary during deposition, is used to deposit a nondoped ZnO layer (i-ZnO) and, subsequently, the Al-doped ZnO (ZnO:Al) front contact of the cells in a single run. The ZnO:Al target has a 2% weight of Al_2O_3, and both the ZnO:Al and the i-ZnO target have a purity of 3N. The RF power is 200 W for the i-ZnO layer and 300 W for the ZnO:Al layer. The argon flow during the sputter deposition is 14 sccm, and a throttle valve is used to achieve a sputter pressure close to 0.133 Pa. There is an additional flow of oxygen of 5 sccm present under ignition and target conditioning. The diameters of both of the targets are 125 mm, which limit the maximum substrate size to 5 × 5 cm^2 for reasonably uniform ZnO layers. The highly resistive i-ZnO layer in our baseline devices has a typical thickness of 90 ± 10 nm, when deposited on a glass substrate. The thickness of the ZnO:Al front contact when deposited directly on a glass substrate is 350 ± 20 nm, and the sheet resistance is 30 ± 10 Ω/square. The i-ZnO layer gives a lower number of shunted cells and reduces the influence of electrical inhomogeneities over the area for devices with the CdS buffer layer [8]–[10]. In contrast, high-performance cells without the i-ZnO layer have been obtained when using the $Zn_{1-x}Sn_xO_y$ and the Zn(O,S) [7], [11]. However, all devices in this paper contain an i-ZnO layer.

F. Grid Deposition

After the deposition of the front contact, a metal grid is deposited on the cells to facilitate the current collection and provide a contact pad for current–voltage (*J*–*V*) characterization of the cells. The grid is built up by a Ni/Al/Ni stack deposited by evaporation where the grid pattern is defined using an aperture mask. The function of the two thin nickel layers is to prevent the aluminum to react with oxygen from the front contact and from air, respectively. The second nickel layer also facilitates an ohmic contact between the grid and the measuring probes. The evaporation system used for the grid deposition is a Balzers BA510 that contains an electron-beam heated evaporation source with

multiple crucibles mounted on a turntable. The evaporation rate and film thickness are monitored with a quartz-crystal microbalance. The total grid thickness is 3000 ± 500 nm. Sheet resistance measurements on nonstructured grid layers deposited on a glass substrate give values between 0.01 and 0.02 Ω/square.

G. Patterning

To define the 0.5-cm^2 cell areas, mechanical scribing with a stylus is used. Mini-modules with an aperture area of up to 12.5 cm × 12.5 cm can be fabricated. In this study, a 4 × 4 cm^2 module is presented that is patterned to have ten series-connected cells with a cell width of 4 mm to optimize the output at the standard test condition irradiance of 1000 W/m^2 [12]. First, the Mo back-contact layer is patterned into individual cells by direct induced ablation through the glass substrate using a frequency-doubled, pulsed Nd:YVO_4 laser with a wavelength of 532 nm and 10-ns pulse length, forming 50-μm-wide P1 lines [13]. The patterned substrate is covered with CIGS and a buffer layer according to the cell process described previously. After deposition of the i-ZnO layer, the process sequence is interrupted for the P2 step. Here, a trench through the deposited layers down to the Mo back contact is opened adjacent to the P1 lines by mechanical scribing with a stylus. The ZnO:Al front contact is deposited, and, finally, the P3 lines are formed adjacent to the P2 lines. The P3 lines provide electrical isolation of the front contacts of neighboring cells by mechanical removal of the whole stack of deposited layers down to the Mo back contact with the stylus. The mechanical scribe lines have rough edges due to chipping, and the widths of the P2 and P3 lines are just below 150 μm and up to 300 μm, respectively [13].

H. Antireflective Coating

An antireflective (AR) coating is deposited on best devices or to avoid interference fringes, e.g., when window layers with different thicknesses are compared. The 105 ± 5-nm-thick MgF_2 layer is evaporated from a resistively heated baffled box source. Adding the AR coating typically increases the conversion efficiency of a cell with an additional 1% (absolute), mainly due to an increase in J_{sc}.

I. Device Measurement

For the in-house *J–V* measurements, a tungsten halogen lamp is used. The lamp is calibrated, with a certified silicon photodiode from Hamamtsu Photonics, to give the same amount of photons as in AM 1.5 light at an intensity of 1 kW/m^2. The temperatures of the devices are kept at 25 °C by a Peltier element.

III. Result

The baseline process generates on a regular basis CdS buffer layer samples with average conversion efficiencies (η) between 15.4% and 17.4% without AR coating, as can be seen in Fig. 3. Recently, new record CdS and $Zn_{1-x}Sn_xO_y$ buffer layer cells have been made and the highest certified η achieved (with AR coating) is now 18.6% for a cell with the CdS buffer layer and 18.2% for a cell with the $Zn_{1-x}Sn_xO_y$ buffer layer. The *J–V*

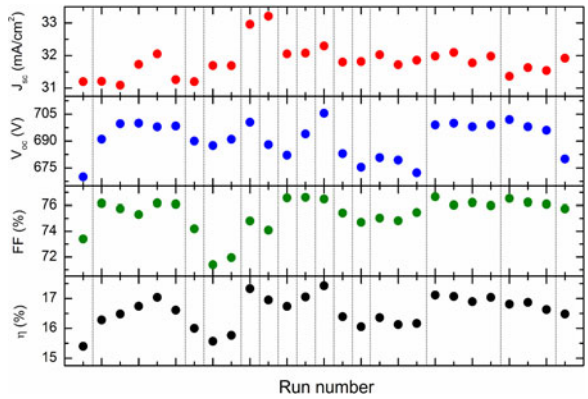

Fig. 3. Average *J–V* values for 27 different samples with the CdS buffer layer manufactured by the ÅSC baseline since the start of 2011. Samples in between two dashed lines have CIGS from the same run.

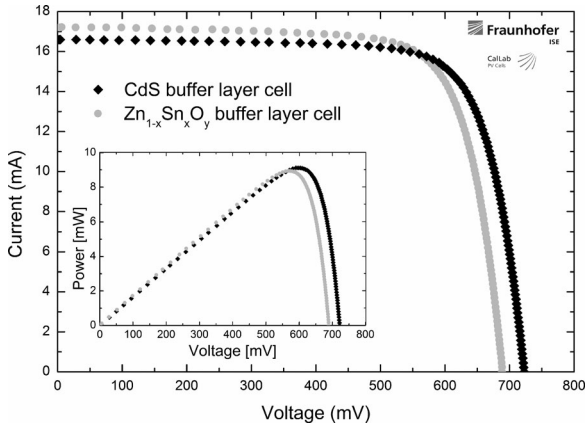

Fig. 4. *J–V* curves for an SLG/Mo/CIGS/CdS/i-ZnO/ZnO:Al/MgF_2 solar cell and for an SLG/Mo/CIGS/$Zn_{1-x}Sn_xO_y$/i-ZnO/ZnO:Al/MgF_2 solar cell processed with the ÅSC baseline procedure and measured under STC by Fraunhofer ISE CalLab PV Cells. The inset shows the corresponding power–voltage curves.

characteristics, as measured by the Fraunhofer ISE CalLab PV Cells, of these two cells are found in Table II, and the corresponding *J–V* curves are displayed in Fig. 4. Corresponding external quantum efficiency (EQE) curves, which are also measured by Fraunhofer ISE CalLab PV Cells, of the two cells are presented in Fig. 5.

A mini-module with the CdS buffer layer has also been made for this paper, following the exact same procedure as for the cells with exception of the pattering steps and that no grid was deposited on the module. The *J–V* characteristics of this 16.8% efficient 15.6-cm^2 mini-module are found in Table II.

Our own measurements on the two cells made by the tungsten halogen lamp agree well with the measurements done by the Fraunhofer ISE CalLab PV Cells. Especially, the open-circuit voltage (V_{oc}) is in good agreement, whereas our measurement setup slightly overestimates both the short-circuit current (J_{sc}) and fill factor (FF) by approximately 1–2% (relative) leading to marginally higher conversion efficiencies, which is well within the measurement errors of the Fraunhofer ISE CalLab PV Cells measurements.

TABLE II
J–V CHARACTERISTICS FOR THE ÅSC GROUPS RECORD CELLS AND MODULE

Sample	Area [cm^2]	V_{oc} [mV]	I_{sc} [mA]	J_{sc} [mA/cm^2]	FF [%]	η[%]
CdS buffer layer cell [a]	0.4917 ± 0.0061	722.7 ± 3.6	16.60 ± 0.41	33.76 ± 0.94	76.09 ± 0.76	18.56 ± 0.60
$Zn_{1-x}Sn_xO_y$ buffer layer cell [a]	0.4907 ± 0.0061	688.7 ± 3.4	17.21 ± 0.43	35.07 ± 0.98	75.30 ± 0.75	18.19 ± 0.59
Zn(O,S) buffer layer cell [b]	0.5	0.689	-	35.511	75.77	18.53
CdS buffer layer module [a]	15.578 ± 0.031	7119 ± 36	52.4 ± 1.3	-	70.08 ± 0.70	16.78 ± 0.50

[a]The samples are fabricated for this paper. The measurements were done at Standard Testing Conditions (Total Irradiance: 1000 W/m^2, Temperature: 25 °C and Spectral Irradiance distribution: AM 1.5G Ed.2 (2008)/3/) with a four-quadrant power amplifier and a set of Burster calibration resistors at the Fraunhofer ISE CalLab PV Cells.
[b]A previous result [14] that was independently measured at the National Renewable Energy Laboratory.

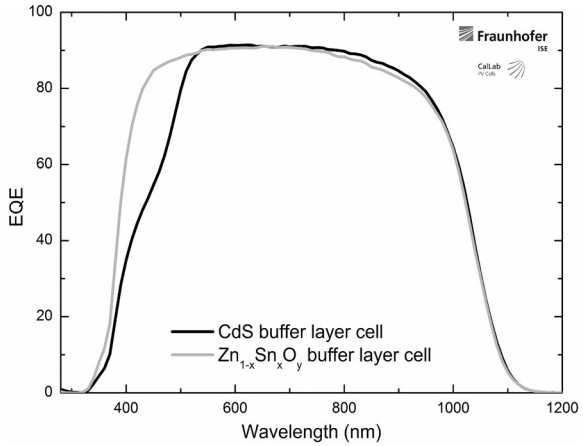

Fig. 5. EQE comparison between the two record cells processed by the ÅSC baseline procedure.

IV. DISCUSSION

A CIGS deposition system with three sources has a limited freedom to vary the evaporation rate profiles. The aim with our source configuration is to get a built-in gallium grading to enhance carrier collection, but to limit the absorption losses caused by a high Ga concentration at the back of the solar cell. We note that the deposition profile in Fig. 1 agrees well with the resulting SIMS depth profile in Fig. 2, and that there is no large diffusion of Cu in our CIGS layers. Previously published results using a similar profile (with AR coating) were 16.7% ($V_{\rm oc}$ = 654 mV, $J_{\rm sc}$ = 33.3 mA/cm^2, FF 76.5%) [15]. The gain of almost 2% (absolute) is primarily obtained in improved voltage, although a similar average [Ga]/([Ga]+[In]) ratio has been used. The improvements that have led to the voltage increase are several and are discussed below.

The overall stability of the baseline has been improved with the changes discussed below. In [15], the discrepancy in efficiency between different samples in a single run in the CIGS evaporator is stated to vary between 12.6% and 15.7%, i.e., 3.1% (absolute) difference. As can be seen in Fig. 3, the discrepancy in the current baseline process between samples made in separate CIGS deposition runs is within 2% (absolute). The variation between samples made in the same CIGS deposition run is usually below 0.3% (absolute). It should be noted that the reproducibility of the baseline process presented in Fig. 3 is a combination of the reproducibility of all process steps.

Introduction of individual control of the substrate heaters has allowed an optimization of the temperature profile in the inline co-evaporation process. In addition, the metal source control has been upgraded with dc power supply, which has greatly enhanced the rate stability and reduced the ramp-up and stabilization time. It is likely that this is the major reason for the high reproducibility discussed previously. As seen in Fig. 5, the EQE response in the near-IR part of the spectrum is high, which is indicative of a high carrier collection. However, there is a slightly lower slope near the bandgap absorption edge as compared with CIGS without a Ga gradient, leading to a small absorption loss. The losses caused by profiles with linear grading are further discussed in [16]. We conclude that there is still room for improvement of the [Ga]/([Ga]+[In]) profile.

Some issues that have been addressed are related to improving the Mo quality, where mainly the Na transport properties are improved, as discussed in [17]. Another issue is related to the removal of elemental selenium that might be found on the CIGS surface after the CIGS deposition [18], and this has been a part of the optimization process that leads to the higher efficiencies. Elemental selenium in small amount is easily removed by a post-treatment in vacuum, where samples are heated for a short time. Preheating is part of the ALD deposition, but not of the CBD-CdS process, where elemental selenium at the interface was identified as a cause of interface problems, which led to reduced voltage and FF. Small amounts of crystalline selenium were found to influence the interface properties, as discussed in [19]. Also related to the CIGS/buffer interface properties is the fact that the buffer layers are deposited within 5 min after unloading of the samples from vacuum. Previously, the air exposure time could extend up to 12 h. The deposition time of the CdS buffer layer has been increased leading to a thicker layer and slightly increased parasitic loss in the blue part of the EQE graph in Fig. 5. In our case, the slightly longer deposition time has been found to increase the process window and improve the robustness of the baseline at the expense of a slight current loss.

The difference between the CdS and the $Zn_{1-x}Sn_xO_y$ buffer layer in *J–V* characteristics is well illustrated in Fig. 4. The $Zn_{1-x}Sn_xO_y$ buffer layer yields higher $J_{\rm sc}$, but lower $V_{\rm oc}$, and slightly lower FF. The higher current is due to the higher mobility gap of $Zn_{1-x}Sn_xO_y$ compared with CdS, which leads to a higher EQE response in the UV-blue region, which is clearly illustrated in Fig. 5. The current generation in the short wavelength part of the spectrum is thereby limited by the front contact in cells with the $Zn_{1-x}Sn_xO_y$ buffer layer, rather than by the buffer layer,

which is the case for the CdS cells [7]. The lower V_{oc} and FF values that are obtained for cells with the $Zn_{1-x}Sn_xO_y$ buffer layers as compared with the cells with CdS probably originate from a different buffer/CIGS interface, possibly due to the air exposure between the CIGS and $Zn_{1-x}Sn_xO_y$ deposition leading to oxides which are not removed during the ALD process. In the CdS process, some pretreatment of the CIGS surface takes place in the ammonia-containing solution [6]. It is likely that even higher efficiencies for $Zn_{1-x}Sn_xO_y$ buffer layer cells can be reached if the samples could be transferred without vacuum breach from the CIGS evaporation chamber to the $Zn_{1-x}Sn_xO_y$ ALD system.

V. Conclusion

The ÅSC CIGS solar cell baseline process has been improved throughout the years, both in efficiency, and also in robustness and process yield. The current baseline efficiency level is 15.4–17.4% conversion efficiency prior to AR coating. Two record cells, one with a standard CdS buffer layer and one with a $Zn_{1-x}Sn_xO_y$ buffer layer developed at the ÅSC, have been measured by the Fraunhofer ISE to have conversion efficiencies of 18.6% and 18.2%, respectively. The CIGS layers have been deposited in a single-step inline co-evaporation process with 17.5-min deposition time and with the limitation of using only four evaporation sources. The CIGS layers exhibit a linear [Ga]/([Ga]+[In]) profile and, thereby, a linear bandgap grading going from 1.14 eV at the front contact to 1.38 eV at the back contact.

References

[1] J. Kessler, D. Schmid, S. Zweigart, H. Dittrich, and H. W. Schock, "$CuInSe_2$ film formation from sequential depositions of In(Se):Cu:Se," in *Proc. 12th Eur. Conf. Photovoltaic Sol. Energy Conf.*, Amsterdam, The Netherlands, 1994, pp. 648–652.

[2] S. Schleussner, U. Zimmermann, J. T. Wätjen, K. Leifer, and M. Edoff, "Effect of gallium grading in Cu(In,Ga)Se_2 solar-cell absorbers produced by multi-stage coevaporation," *Sol. Energ. Mater. Sol. C.*, vol. 95, pp. 721–726, 2011.

[3] M. Powalla, G. Voorwinden, D. Hariskos, P. Jackson, and R. Kniese, "Highly efficient CIS solar cells and modules made by the co-evaporation process," *Thin Solid Films*, vol. 517, pp. 2111–2114, 2009.

[4] M. I. Alonso, M. Garriga, C. A. Durante Rincón, E. Hernández, and M. León, "Optical functions of chalcopyrite $CuGa_xIn_{1-x}Se_2$ alloys," *Appl. Phys. A.*, vol. 74, pp. 659–664, 2002.

[5] D. Regesch, L. Gütay, J. K. Larsen, V. Deprédurand, and D. Tanaka, "Degradation and passivation of $CuInSe_2$," *Appl. Phys. Lett.*, vol. 101, pp. 112108-1–112108-4, 2012.

[6] D. Lincot, R. Ortega-Borges, J. Vedel, M. Ruckh, J. Kessler, K. O. Velthaus, D. Hariskos, and H. W. Chock, "Chemical bath deposition of CdS on $CuInSe_2$: Combining dry and wet processes for high efficiency thin film solar cells," in *Proc. 11th Eur. Photovoltaics Sol. Energy Conf.*, Montreux, Switzerland, 1992, pp. 870–873.

[7] J. Lindahl, J. T. Wätjen, A. Hultqvist, T. Ericson, M. Edoff, and T. Törndahl, "The effect of $Zn_{1-x}Sn_xO_y$ buffer layer thickness in 18.0% efficient Cd-free Cu(In,Ga)Se2 solar cells," *Prog. Photovoltaic: Res. Appl*, doi: 10.1002/pip.2239.

[8] U. Rau and M. Schmidt, "Electronic properties of ZnO/CdS/Cu(In,Ga)Se_2 solar cells—Aspects of heterojunction formation," *Thin Solid Films*, vol. 387, pp. 141–146, 2001.

[9] S. Ishizuka, K. Sakurai, A. Yamada, K. Matsubara, P. Fons, K. Iwata, S. Nakamura, Y. Kimura, T. Baba, H. Nakanishi, T. Kojim, and S. Niki, "Fabrication of wide-gap Cu$(In_{1-x}G_x)Se_2$ thin film solar cells: A study on the correlation of cell performance with highly resistive i-ZnO layer thickness," *Sol. Energy Mater. Sol. C.*, vol. 87, pp. 541–548, 2005.

[10] R. Scheer, L. Messmann-Vera, R. Klenk, and H.-W. Schock, "On the role of non-doped ZnO in CIGSe solar cells," *Prog. Photovoltaic: Res. Appl.*, vol. 20, pp. 619–624, 2011.

[11] A. Hultqvist, C. Platzer-Björkman, T. Törndahl, M. Ruth, and M. Edoff, "Optimization of i-ZnO window layers for Cu(In,Ga)Se_2 solar cells with ALD buffers," in *Proc. 22nd Eur. Photovoltaic Sol. Energy Conf.*, Milan, Italy, 2007, pp. 2381–2384.

[12] J. Johansson, U. Zimmermann, and M. Edoff, "Modeling and optimization of CIGS modules," in *Proc. 22nd Eur. Photovoltaic Sol. Energy Conf.*, Milan, Italy, 2007, pp. 1922–1925.

[13] P.-O. Westin, U. Zimmermann, and M. Edoff, "Laser patterning of P2 interconnect via in thin-film CIGS PV modules," *Sol. Energy Mater. Sol. C.*, vol. 92, pp. 1230–1235, 2008.

[14] U. Zimmermann, M. Ruth, and M. Edoff, "Cadmium-free CIGS mini-modules with ALD-grown Zn(O,S)-based buffer layers," in *Proc. 21st Eur. Photovoltaic Sol. Energy Conf.*, Dresden, Germany, 2006, pp. 1831–1834.

[15] M. Edoff, S. Woldegiorgis, P. Neretnieks, M. Ruth, J. Kessler, and L. Stolt, "CIGS submodules with high performance and high manufacturability," in *Proc. 19th Eur. Photovoltaic Sol. Energy Conf.*, Paris, France, 2004, pp. 1690–1693.

[16] K. Decock, S. Khelifi, and M. Burgelman, "Analytical versus numerical analysis of back grading in CIGS solar cells," *Sol. Energy Mater. Sol. C.*, vol. 95, pp. 1550–1554, 2011.

[17] M. Edoff, N. Viard, T. Wätjen, S. Schleussner, P.-O. Westin, and K. Leifer, "Sputtering of highly adhesive Mo back contact layers for Cu(In,Ga)Se_2 solar cells," in *Proc. 24th Eur. Photovoltaic Sol. Energy Conf.*, Hamburg, Germany, 2009, pp. 3037–3040.

[18] T. Törndahl, E. Coronel, A. Hultqvist, C. Platzer-Björkman, K. Leifer, and M. Edoff, "The effect of $Zn_{1-x}Mg_xO$ buffer layer deposition temperature on Cu(In,Ga)Se_2 solar cells: A study of the buffer/absorber interface," *Prog. Photovoltaic: Res. Appl.*, vol. 17, pp. 115–125, 2008.

[19] C. Platzer-Björkman, P. Zabierowski, J. Pettersson, T. Törndahl, and M. Edoff, "Improved fill factor and open circuit voltage by crystalline selenium at the Cu(In,Ga)Se_2/buffer interface," *Prog. Photovoltaic: Res. Appl.*, vol. 18, pp. 249–256, 2010.

Authors' photographs and biographies not available at the time of publication.